ELSEVIER

Int. J. Miner. Process. 68 (2003) 167–182

INTERNATIONAL JOURNAL OF MINERAL PROCESSING

www.elsevier.com/locate/ijminpro

New method and equations for determining attachment tenacity and particle size limit in flotation

Anh V. Nguyen

Department of Chemical Engineering, The University of Newcastle, Callaghan, New South Wales 2308, Australia

Received 4 February 2002; received in revised form 18 June 2002; accepted 19 June 2002

Abstract

A new method and simple, yet accurate, equations for determining the tenacity of particle attachment and the particle size limit in flotation were developed by applying the force analysis of the gravity–capillarity coupling phenomena controlling the bubble–particle stability and detachment. Approximate solutions to the Young–Laplace equation were used to develop simple equations for the tenacity of attachment of particles with diameter up to 20 mm. Simple equations for the maximum size of floatable particles were derived as explicit functions of the particle contact angle, the surface tension, the particle density and the mean centrifugal acceleration of turbulent eddies. For the typical particle size and contact angle encountered in flotation, the analysis showed that the bubble size has little effect on the tenacity of particle attachment. The prediction for the largest size of floatable particles is compared with the experimental data and signifies influence of turbulence on the particle detachment.

Keywords: particle size; detachment; bubble–particle interaction; coarse-particle flotation; flotation theory

1. Introduction

Particle size is an important parameter in flotation and has been the focus of the flotation research for decades. Flotation recovery of both fine and coarse particles is usually remarkably low, leading to the "elephant" shape of the recovery versus particle size curves. Coarse particles badly float mostly because the bubble–particle aggregates are not strong enough to prevent the particle detachment from the bubble surface caused by the particle weight and turbulence eddies during the rise of the aggregates in the pulp

E-mail address: cgavn@alinga.necastle.edu.au (A.V. Nguyen).

0301-7516/03/$ - see front matter
PII: S0301-7516(02)00069-8

phase to the froth phase and then to the froth launder. Efficiency of the bubble–particle stability depends on the particle size, particle hydrophobicity and external detaching forces. Even in the flotation of fine particles, the bubble–particle detachment can significantly influence the kinetics of flotation taking place in mechanical cells by intensive turbulent agitation (Deglon et al., 1999). For these fine particles, the bubble–particle detachment is usually allegedly neglected.

Unlike the collision and attachment interactions between bubbles and particles, the detachment interaction is not satisfactorily quantified yet. We do not have any satisfactory theory on the bubble–particle stability/detachment, which can explicitly describe the detachment phenomena with the whole range of the particle size although the fundamentals of the bubble–particle stability/detachment were formulated in the early days of flotation (Gaudin, 1939; Kabanov and Frumkin, 1933; Wark, 1933).

In the seventies and eighties, Schulze (1977, 1982, 1983) further advanced the analysis on the forces influencing the particle stability and detachment. It is shown that the bubble–particle detachment is characterised by highly nonlinear equations describing the gravity–capillarity coupling phenomena controlling the stability of the bubble–particle aggregates. These phenomena are, in turn, mathematically described by equations in terms of the particle size, particle density and particle contact angle among many other parameters. The equation for predicting the maximum size of floatable particles, i.e., the upper limit of particle size in flotation, gives (Schulze, 1983)

$$(R_{\mathrm{p\ max}})^2 + R_{\mathrm{p\ max}} \frac{3\sin^2\omega^*(\sigma' - \rho_{\mathrm{l}} g z_{\mathrm{o}})}{4(g\Delta\rho + b_{\mathrm{m}}\rho_{\mathrm{p}})} + \frac{3\sigma\sin\omega^*\sin(\omega^* + \theta)}{2(g\Delta\rho + b_{\mathrm{m}}\rho_{\mathrm{p}})} = 0, \tag{1}$$

where $R_{\mathrm{p\ max}}$ is the maximum radius of floatable particles, ρ_{p} and ρ_{l} are the particle density and the liquid density, respectively, $\Delta\rho = \rho_{\mathrm{p}} - \rho_{\mathrm{l}}$, θ is the particle contact angle, σ is the liquid surface tension, g is the acceleration due to gravity and b_{m} is the mean centrifugal acceleration of turbulent eddies, known as the "machine" acceleration. σ' is the capillary pressure over the three-phase contact and is described by

$$\sigma' = \frac{2\sigma}{R_{\mathrm{b}}} - 2R_{\mathrm{b}}\rho_{\mathrm{l}} g, \tag{2}$$

where R_{b} is the bubble radius. ω^* in Eq. (1) is related to the contact angle by

$$\omega^* = \pi - \frac{\theta}{2}. \tag{3}$$

In Eq. (1), z_0 is the height of the gas–liquid meniscus over the three-phase contact under the condition that the central angle ω (Fig. 1) satisfies Eq. (3), i.e., $\omega = \omega^* = \pi - \theta/2$. In the case of a small three-phase contact radius, z_0 can be determined by inserting $\beta = \theta/2$ into the Derjaguin equation (Derjaguin, 1946; James, 1974) given by Eq. (4). This equation describes the height, H, of the gas–liquid meniscus over the three-phase contact as a function of its radius, r_{tpc}, and its angular inclination, β, to the horizontal axis (Fig. 1).

$$H = r_{\mathrm{tpc}}\sin\beta\left(\ln\frac{4L/r_{\mathrm{tpc}}}{1+\cos\beta} - \gamma\right), \tag{4}$$

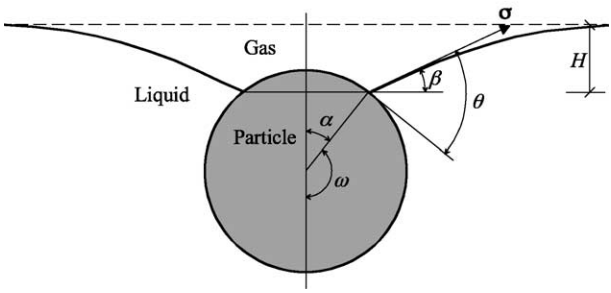

Fig. 1. Notations of a sphere attached to an initially planar gas–liquid interface.

where $\gamma = 0.577$ and is the Euler constant. For the radius of the three-phase contact, we have $r_{tpc} = R_p \sin \omega$. L is the capillary length defined by

$$L = \sqrt{\frac{\sigma}{\rho_l g}}. \tag{5}$$

In general, the height, z_0, of the gas–liquid meniscus in Eq. (1) is a function of the particle radius, and the contact angle and must be obtained from the Young–Laplace equation describing the deformation of the gas–liquid interface.

It can be observed that since the height of the meniscus is a complicated function of the particle radius (see the highly nonlinear Eq. (4), for example), Eq. (1) cannot be explicitly solved for the maximum particle radius. The steps of the successive technique (Schulze, 1983) for solving Eq. (1) include:

Step 1: Neglect the z_0 term and the capillary pressure in Eq. (1), then determine and calculate the first approximate value for $R_{p\ max}$, viz.,

$$R_{p\ max} \cong \sqrt{-\frac{3\sigma \sin\omega^* \sin(\omega^* + \theta)}{2(\Delta\rho + \rho_p b_m)}},$$

Step 2: Calculate the dimensionless horizontal (x) coordinate of the three-phase contact on the particle:

$$x = (R_{p\ max}/L)\sin\omega^*,$$

Step 3: Use the tabulated data (or the approximate expressions) to find the corresponding vertical (y) coordinate of the three-phase contact on the particle. The angular inclination $\beta = \omega^* + \theta - \pi$ is used as the second variable. The required meniscus height z_0 is then determined by $z_0 = yL$.

Step 4: Insert the obtained value of z_0 into Eq. (1) and solve this quadratic equation to obtain a new value of $R_{p\ max}$.

Step 5: Return to Step 2 and repeat the calculation until the desired accuracy is achieved.

This numerical technique has been successfully used for determining the upper particle size limit of flotation for many years. However, in many cases, $R_{p\ max}$ is not the final aim

of the flotation engineering calculation but it is the required input for the next steps of the modelling and simulating exercises. Under these circumstances, the available technique is difficult to employ since it cannot provide any explicit expression for $R_{p\ max}$ and prompted our research reported in this paper.

The results reported in this paper are obtained based on the outcomes of a recent paper (Nguyen, 2002), which develops new analytical solutions to the Young–Laplace equation for the meniscus deformation by the particle attachment applying a combined analytical–empirical approach. To highlight the physical insight of the particle stability and detachment phenomena, the force analysis will briefly be described in the next section. Then the tenacity of the particle attachment to the gas–liquid interface will be analysed and determined. The simple approximate equations for the tenacity will be used to derive simple expressions for the maximum size of floatable particles. Next, the influence of the bubble size on the tenacity and the maximum particle size will be investigated. The determination of the mean centrifugal acceleration of turbulent eddies will be outlined. Finally, the developed equations for determining the maximum size of floatable particles will be compared to the available experimental data.

2. Balance of forces on a sphere attached to a large bubble

For simplicity, we commence with the analysis of forces on a spherical particle attached to a significantly large bubble so that the local bubble–particle geometry can be approximated to the geometry of the attachment of a sphere to an initially planar gas–liquid interface. The geometry of this system is depicted in Fig. 1. Detailed description of the forces on the particle in Fig. 1 is available in Schulze (1983). However, for better understanding, the forces on the attached particle are briefly summarised below.

One of the most important forces is the *capillary force*, which acts along the tangent to the gas–liquid interface at the three-phase contact line and tends to pull the particle into the gas phase. This force is, therefore, an effective force for stabilising the particle attachment to the gas–liquid interface. The magnitude of this force is equal to the product of the gas–liquid surface tension, σ, and the length, $2\pi r_{tpc}$, of the three-phase contact with radius r_{tpc}. The surface tension can be resolved into the vertical and horizontal forces. Due to the rotational symmetry along the vertical axis, the horizontal component of the capillary force vanishes and only the vertical component retains. Expressing r_{tpc} in terms of α and the particle radius, R_p, and β in terms of α and θ, we obtain the frequently used expression for the capillary force, viz.,

$$F_c = 2\pi R_p \sigma \sin\alpha \sin(\theta - \alpha). \tag{6}$$

The second force, which supports the particle attachment to the interface, is the *buoyancy*, F_b, of the particle volume immersed in the liquid phase. This force can be described by

$$F_b = \frac{\pi R_p^3 \rho_l g}{3}(2 + 3\cos\alpha - \cos^3\alpha), \tag{7}$$

where $\pi R_p^3(2+3\ \cos\alpha-\cos^3\alpha)/3$ is the volume of the liquid phase displaced by the particle.

The third force, which also stabilises the particle attachment to the gas–liquid interface, is the *pressure force*, F_p, coming from the hydrostatic pressure over area enclosed by the three-phase contact line. This hydrostatic pressure force is described by Eq. (8), i.e.,

$$F_p = \pi R_p^2 H \rho_l g \sin^2\alpha, \tag{8}$$

where H is the depth of the deformed gas–liquid interface at the three-phase contact line (see Fig. 1) and $\pi R_p^2 H\ \sin^2\alpha$ is the volume of the cylinder over the area, πr_{tpc}^2 of the three-phase contact.

The other relevant force on the particle is the *particle weight*, F_g, which pulls the attached particle into the liquid phase. We obtain

$$F_g = -\frac{4\pi R_p^3 \rho_p g}{3}. \tag{9}$$

Since the positive direction is taken opposite to the direction of the acceleration due to gravity, the minus sign on the right-hand side of Eq. (9) indicates that the particle weight is directed downward.

In summary, we identify four (static) forces on the particle attached to an initially planar surface, namely, the capillary force, the buoyancy of the particle volume immersed in the liquid, the hydrostatic pressure force and the particle weight. Equilibrium is obtained if

$$F_c + F_b + F_p + F_g = 0. \tag{10}$$

Rewriting the particle volume immersed in the liquid phase by the total particle volume less the particle volume in the gas phase, we can convert Eq. (10) into a useful expression for the force balance, i.e.,

$$2\pi R_p \sigma \sin\alpha \sin(\theta-\alpha) - \frac{\pi R_p^3 \rho_l g}{3}(2-3\cos\alpha+\cos^3\alpha) + \pi R_p^2 H \rho_l g \sin^2\alpha = \frac{4\pi R_p^3 g \Delta\rho}{3}. \tag{11}$$

Principally, this equation can be solved for the maximum size of floatable particles if the position of the three-phase contact on the particle with the maximum size is known. However, this usually leads to an equation similar to Eq. (1), which contains the transcendent function, $H(R_p)$, of the height of the deformed meniscus. Therefore, no explicit expression for the particle size can be obtained as highlighted in the Introduction. The new development is outlined below.

It can be observed that the left-hand side of Eq. (11) describes the forces, which are functions of the position of the three-phase contact. As most of these forces support the

adhesion of the particle onto the interface, they are jointly referred to as the adhesive force and are described by F_{ad}, for which we have

$$F_{ad} = 2\pi R_p \sigma \sin\alpha \sin(\theta - \alpha) + \pi R_p^2 H \rho_l g \sin^2\alpha - \frac{\pi R_p^3 \rho_l g}{3}(2 - 3\cos\alpha + \cos^3\alpha). \quad (12)$$

The dependence of the adhesive force on the position of the three-phase contact on the particle is described in the next section.

It is also worth noting that the right-hand side of Eq. (11) describes the weight of the particle less its buoyancy. This apparent weight of the particle in the liquid phase is independent of the position of the three-phase contact on the particle. As these forces tend to detach the particle from the bubble surface, they are jointly called the *detaching force* and are described by F_{de}. The detaching force may have additional components, including the force due to the acceleration of turbulent eddies, readily considered in Eq. (1). Applying Schulze's approach, the generic expression for the detaching force can be described by

$$F_{de} = \frac{4\pi R_p^3 \Delta\rho}{3}(g + b_m). \quad (13)$$

Comments on whether $\Delta\rho$ or ρ_p should be used in the determination of the force due to the turbulent eddies appeared in Eq. (13) are available in (Schulze, 1983). Here, we use $\Delta\rho$ since it can be a good approximation for both light and heavy particles.

3. Tenacity of the particle attachment

The stable attachment of particles to the gas–liquid interface depends strongly on the hydrophobic nature of the particles: The more hydrophobic the surface of the particle, the more stably it attaches to the interface. This influence now can be examined by analysing Eq. (12).

The typical dependence of the adhesive force described Eq. (12) on the three-phase contact position described in terms of central angle α is shown in Fig. 2. In the calculation of the adhesive force, the meniscus depression, H, is explicitly determined as a function of the radius of the three-phase contact and the meniscus inclination by the approximate solutions recently available for the whole range of the three-phase radius (Nguyen, 2002). By using the approximate solutions, the variation of the adhesive force given by Eq. (12) versus the location of the three-phase contact on the particle surface can be derived without any significant numerical computational resources. This significantly enhances the analysis presented in this paper.

As can be seen from Fig. 2, with the increase in α from zero, the adhesive force increases, reaching a maximum and then decreases. It is noteworthy that the maximum force is a stable property of the meniscus–particle system that can be approached, at least

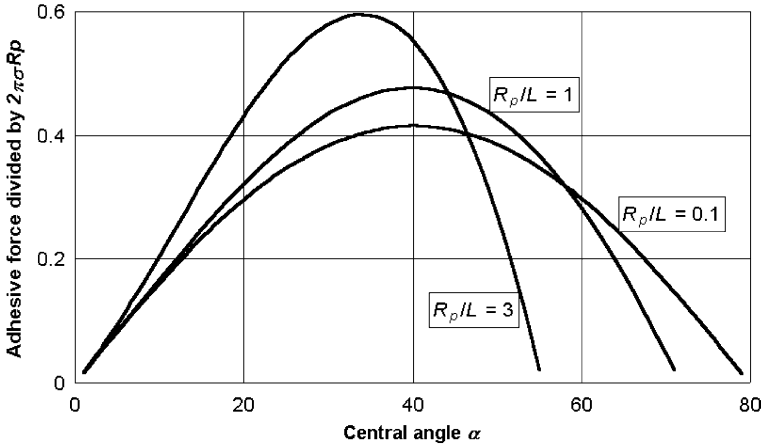

Fig. 2. Adhesive force described Eq. (12) versus the central angle α at $\theta = 80°$.

in theory, from both sides of the adhesive force curve. The loci of the three-phase contact of maximum adhesive force are described by

$$\left(\frac{dF_{ad}}{d\alpha}\right)_{\alpha=\alpha_m} = 0, \tag{14}$$

where α_m determines the location of the three-phase contact of the maximum adhesive force. The position of the maximum of the adhesive force has to be determined from this equation.

To determine the tenacity of the particle–meniscus contact, the equilibrium condition of forces on the particle attached to the gas–liquid interface described by Eq. (11) is necessary but not sufficient. The tenacity, T, of the particle–meniscus contact is determined by the maximum adhesive force because the particle is detached from the meniscus if the detaching force exceeds the magnitude of the maximum adhesive force (see the next section). The expression for the tenacity can be obtained by replacing α in Eq. (12) by α_m. It gives

$$T = 2\pi R_p \sigma \sin\alpha_m \sin(\theta - \alpha_m) + \pi R_p^2 H \rho_l g \sin^2\alpha_m - \frac{\pi R_p^3 \rho_l g}{3}(2 - 3\cos\alpha_m + \cos^3\alpha_m). \tag{15}$$

The criterion equation for α_m, derived from Eq. (14), gives

$$\cos(\theta - 2\alpha_m) + \left(\frac{R_p}{L}\right)^2 \left[\frac{d}{d\alpha_m}\left\{\frac{H(\alpha_m)}{R_p}\sin^2\alpha_m\right\} - \sin^3\alpha_m\right] = 0. \tag{16}$$

Solving Eq. (16) numerically for α_m and inserting the results into Eq. (15), we obtain the dependence of the tenacity of particle attachment on contact angle θ and particle radius R_p. The obtained results for this dependence are shown in the log–log diagram in Fig. 3. For

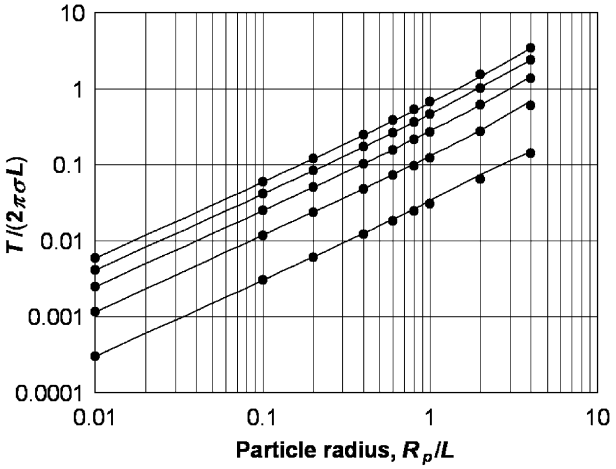

Fig. 3. Tenacity of particle attachment scaled by dividing by capillary force, $2\pi\sigma L$, versus the particle radius scaled by dividing by the capillary length, L, and the particle contact angle ($\theta = 20°$, 40°, 60°, 80° and 100° upward view). Points and solid lines describe the data of the exact and approximate solutions given by Eqs. (15) and (17), respectively.

the given range of contact angles, the slope of the curves of T versus R_p in the log–log diagram is almost constant. Therefore, Eq. (15) can be replaced by Eq. (17), viz.,

$$T = \pi R_p \sigma (1 - \cos\theta)\left\{1 + 2c \times \frac{R_p}{L}\right\}. \tag{17}$$

In Eq. (17), c is the numerical constant ($2c$ is used for later convenience) and can be obtained by the best fit to the numerical results. For the contact angle up to 100° and the particle radius $R_p/L \leq 4$, the best fit gives $c = 0.058$. Taking the usual value $L = 2.7$ mm, the range of applicability of Eq. (17) gives $R_p \leq 10.8$ mm, which can be met in the actual froth flotation and many other specially designed flotation processes, including the film (skin) flotation. For fine particles, $R_p/L \ll 1$ and the maximum adhesive force described by Eq. (17) reduces into

$$T = \pi R_p \sigma (1 - \cos\theta) + O\{(R_p/L)^2\}, \tag{18}$$

which is equal to the maximum capillary force described by Eq. (6). In this limit, the criterion Eq. (16) gives

$$\alpha_m = \theta/2. \tag{19}$$

It can be concluded at this point that the tenacity of particle attachment to the meniscus in flotation is dominated by the particle size, the tension of the gas–liquid interface and the particle contact angle.

4. Maximum size of floatable particles

Note that although the maximum adhesive force can be approached from both sides of the adhesive force versus α curve (Fig. 2), only the right-hand side of the curves (i.e., $\alpha \geq \alpha_m$) represents the stable attachment of particles because any perturbation in the three-phase contact radius (area) on this side caused by external disturbances will return to equilibrium. If the external disturbances are so strong that the maximum adhesive force (the tenacity of attachment) is exceeded, the equilibrium cannot be resumed and the particle will be detached. This situation occurs only on the left-hand side of the adhesive force versus α curve. The stability of particle attachment is, therefore, mathematically described by

$$\begin{cases} T \geq F_{de} \\ \alpha \geq \alpha_m \end{cases}. \tag{20}$$

Now, the maximum size of floatable particles can be found from Eq. (20) by equating the tenacity of attachment to the detaching force, resulting in

$$(R_{p\ max})^2 - \frac{3\sigma(1-\cos\theta)}{4\Delta\rho(g+b_m)}\left(1 + 2c\frac{R_{p\ max}}{L}\right) = 0. \tag{21}$$

Solving the above described quadratic equation for the maximum radius of floatable particles gives

$$\frac{R_{p\ max}}{L} = \frac{3\rho_f g(1-\cos\theta)}{4\Delta\rho(g+b_m)}\left\{c + \sqrt{c^2 + \frac{4\Delta\rho(g+b_m)}{3\rho_f g(1-\cos\theta)}}\right\}. \tag{22}$$

It can be seen that the maximum size of floatable particles is a function of the particle contact angle, the particle density and the centrifugal acceleration of turbulent eddies. As the machine acceleration is of the order of ten to hundred g units in the actual flotation process, the turbulent flow will influence the maximum size of floatable particles most significantly.

Since in the minerals flotation we have $\Delta\rho \gg 0$ and the numerical constant c (which is equal to about 0.058) is smaller than the second term in the square root, we may neglect c in Eq. (22) and obtain a simplified expression for the maximum size of floatable particles, i.e.,

$$R_{p\ max} = \sqrt{\frac{3\sigma(1-\cos\theta)}{4\Delta\rho(g+b_m)}}. \tag{23}$$

This simple equation is accurate for small particles encountered in the actual flotation. For coarser particles and/or light particles, Eq. (22) can give a better estimation for the maximum particle size.

5. Influence of the bubble size

The analysis described in the preceding sections is based on the assumption that the bubble size is significantly (infinitely) large and has no influence on the particle detachment. The influence of the bubble size is now examined.

The geometry of the particle attachment to the bubble is schematically shown in Fig. 4. Except Eq. (8) for the hydrostatic pressure force, the other equations for the forces on the attached particle in Section 2 can be used for the case shown in Fig. 4. As the first approximation, the force due to the pressure over the area enclosed by the three-phase contact is determined by Eq. (24), i.e.,

$$F_p = \pi R_p^2 \sin^2\alpha \left(\rho_l g H - \frac{2\sigma}{R_b} \right). \tag{24}$$

In the limit of $R_b \to \infty$ (infinitely large bubble), Eq. (24) reduces into Eq. (8). The height, H, of the three-phase contact in Eq. (24) is also a function of the bubble radius (see Fig. 4). It can be approximately determined by

$$H = R_b(1 + \cos\varphi), \tag{25}$$

where φ is the central angle at the bubble centre, subtended by the one-half of the gas–solid interface as shown in Fig. 4. This angle is related to the central angle at the particle centre, α, by

$$R_b \sin\varphi = R_p \sin\alpha. \tag{26}$$

From these two equations we obtain

$$H = R_b \left\{ 1 + \sqrt{1 - \left(\frac{R_p}{R_b} \right)^2 \sin^2\alpha} \right\}. \tag{27}$$

Following the procedure described in Section 2, we obtain, with some algebra, the following equation for the adhesive force:

$$\frac{F_{ad}}{2\pi L\sigma} = \frac{R_p}{L}\sin\alpha\sin(\theta - \alpha) - \left(\frac{R_p}{L} \right)^3 \frac{2 - 3\cos\alpha + \cos^3\alpha}{6} + \left(\frac{R_p}{L} \right)^2 \left(\frac{R_b}{L} - \frac{L}{R_b} \right) \sin^2\alpha - \frac{\frac{R_p}{2R_b}\left(\frac{R_p}{L} \right)^3 \sin^4\alpha}{1 + \sqrt{1 - (R_p/R_b)^2 \sin^2\alpha}}. \tag{28}$$

The typical variation of the adhesive force versus the central angle, α, is shown in Fig. 5 for $\theta = 60°$, $R_p = 75$ μm and $R_b = 750$ μm. The capillary length, L, and the surface tension, σ, take the usual values of 2.7 mm and 70 mN, respectively. It can be seen from this figure that with the decrease in the central angle, the adhesive force increases, reaches a maximum at $\alpha = \alpha_m$ and then decreases. As long as the equilibrium described by Eq.

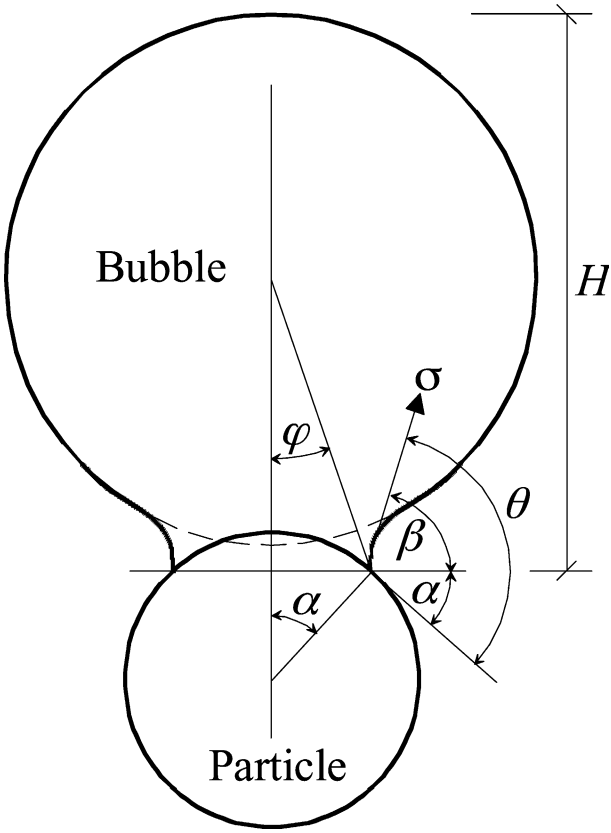

Fig. 4. Geometry of the particle attached to a bubble (not to scale).

(28) is stable, every external disturbance causing any possible detaching force with a magnitude up to the maximum adhesive force is counterbalanced by the internal reactions of the bubble–particle system. Therefore, the maximum adhesive force is a stable property

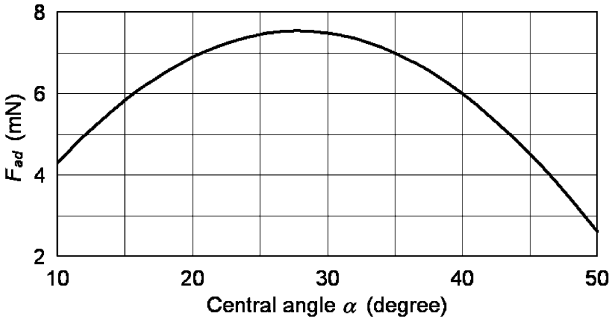

Fig. 5. Adhesive force described by Eq. (28) versus the central angle for $\theta = 60°$, $R_p = 75$ μm and $R_b = 750$ μm.

of the meniscus–particle system that can be approached from the right side of the force curve as described in Section 3. Here the stable position on the right side corresponds to $\alpha \geq \alpha_m$. The tenacity of the three-phase contact is described by the maximum adhesive force and is to be determined by the criterion Eq. (14).

In the actual flotation, we have $R_p/L \ll 1$ and $R_p/R_b \ll 1$. As a result, the second and fourth terms in Eq. (28) have little effect on α_m Inserting Eq. (28) into the criterion Eq. (14), we obtain Eq. (29), i.e.,

$$\sin(\theta - 2\alpha_m) + \left(\frac{R_b R_p}{L^2} - \frac{R_p}{R_b}\right)\sin 2\alpha_m + O\left\{(R_p/L)^2\right\} = 0. \tag{29}$$

Solving Eq. (29) for α_m gives

$$\alpha_m = \frac{1}{2}\arcsin\left\{\frac{\sin\theta}{\sqrt{1 + 2A\cos\theta + A^2}}\right\}, \tag{30}$$

where

$$A = \frac{R_p}{R_b} - \frac{R_b R_p}{L^2}. \tag{31}$$

The tenacity of the bubble–particle contact can be determined by inserting Eq. (30) into Eq. (28). Neglecting the last two terms in the case of $R_p/L \ll 1$, we obtain, after arrangement,

$$T = \pi R_p \sigma\left(\sqrt{1 + 2A\cos\theta + A^2} - \cos\theta - A\right) + O\left\{(R_p/L)^3\right\}. \tag{32}$$

Since and $R_p/R_b \leq 0.1$ and $R_b/L \leq 1$, A is usually smaller than 0.1. Variation of the tenacity of particle attachment to an air bubble versus the contact angle and the bubble and particle sizes is shown for $A = 0$ and 0.09 ($R_p/R_b = 0.1$) in Fig. 6. It can be seen that the bubble size has a very little effect on the tenacity of the particle attachment to the bubble. In particular, in the case of small particles attached to big bubbles and the contact angle

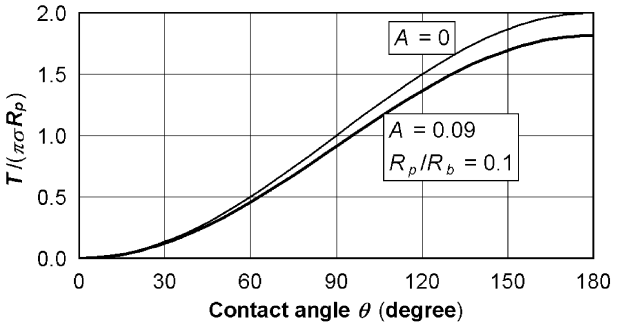

Fig. 6. Tenacity of the particle attachment to an air bubble versus the contact angle. Thin and thick solid lines describe Eqs. (33) and (32), respectively.

$\theta < 90°$, the effect of the bubble size can be neglected. Consequently, Eqs. (30) and (32) can be simplified by replacing $A = 0$, giving

$$T = \pi R_p \sigma (1 - \cos\theta), \tag{33}$$

$$\alpha_m = \theta/2. \tag{34}$$

These equations are the same as Eqs. (18) and (19) described in Section 3, highlighting the fact that for the particle and bubble sizes typically encountered in flotation, the tenacity of particle attachment significantly depends on the particle size, the surface tension and the contact angle and is independent of the bubble size. Thus, the maximum size of floatable particles in the actual flotation can be determined by Eq. (23).

It should be noted that for simplicity, the above described analysis is carried out with the assumption of the spherical shape of the bubbles. The same results, as given by Eqs. (34) and (33), can be obtained with bubbles having a spheroidal shape. In this case, Eq. (27) has to be recast considering that the bubbles now have two semi-axes, instead of the actual bubble radius R_b.

6. Comparison to experimental data and discussion

Comparison between the theory developed in this paper and the experimental data (Schulze, 1980) is shown in Table 1. The experimental results were obtained from the laboratory-scale flotation experiments in a 64-L cell with double-finger impeller and baffles (Bischofberger and Schubert, 1978). The density of the sylvinite particles and the liquid (salt) solution is about 2000 and 1300 kg/m^3, respectively. The surface tension is about 70 mN/m. The contact angle is about 60°. The energy input or the mean turbulent energy dissipation rate ($\bar{\varepsilon}$) was measured in each experiment.

The mean centrifugal acceleration of turbulent eddies b_m is determined by the mean-squared value of the difference in the turbulent fluctuating velocities, W', between two points apart by Δr. As the first approximation, it can be described by Eq. (35) (Schulze, 1983, 1992), i.e.,

$$b_m = \frac{\overline{(\Delta W')^2}}{\Delta r}. \tag{35}$$

For the typical size of the bubble–particle aggregate in flotation, the inertial subrange of the microturbulence theory can be used and gives (Schubert, 1999)

Table 1
Comparison between Eq. (23) and the experimental data (Schulze, 1980) for the maximum size of floatable sylvinite particles

$\bar{\varepsilon}$ (W/kg)	ε_{max} (W/kg)	b_m in the g unit Eq. (39)	$R_{p\ max}$ (μm)	
			Eq. (23)	Experimental
0.43	4.3	4.45	708	700
1.0	10	8.75	529	480
1.5	15	12.10	457	430

$$\sqrt{\overline{(\Delta W')^2}} = 1.38(\varepsilon \Delta r)^{1/3}. \tag{36}$$

When applying Eqs. (35) and (36) to the bubble–particle aggregate stability, we can substitute the (maximum) stable diameter, D_{agr}, of the bubble–particle aggregate for Δr and the local maximum energy dissipation rate (i.e., the average energy dissipation rate in the rotor–stator zone) for ε. We obtain

$$b_m = \frac{1.9(\varepsilon_{max})^{2/3}}{(D_{agr})^{1/3}}, \tag{37}$$

where ε_{max} is the average energy dissipation rate in the rotor–stator zone. For the maximum stable aggregate size in the inertial subrange, we have (Schubert, 1999)

$$D_{agr} = (We)^{3/5}(\sigma/\rho_f)^{3/5}(\varepsilon_{max})^{-2/5}, \tag{38}$$

where *We* is the critical Weber number of the bubble–particle aggregate stability. Inserting Eq. (38) into Eq. (37) we obtain

$$b_m = \frac{1.9(\varepsilon_{max})^{4/5}}{(We)^{1/5}(\sigma/\rho_f)^{1/5}}. \tag{39}$$

In general, the critical Weber number in Eq. (39) must be experimentally determined, but for estimation for flotation systems one can assume $We^{1/5} = 1$.

The local maximum values of the turbulent energy dissipation rate are many times higher than the mean dissipation rate (i.e., about 10–30 times in agitation tanks) (Schubert, 1999). For the flotation cell used to obtain the experimental data given in Table 1, the measurements indicate that the actual dissipation rate at the radial position of 1.3 times radius of the impeller in the rotor–stator zone is about nine times higher than the mean value. A further rapid increase in the local dissipation rate toward the impeller can be extrapolated (Schubert, 1999). Thus, the estimation for $\varepsilon_{max} = 10\bar{\varepsilon}$ used in determining the theoretical results given in Table 1 appears reasonable.

As can be seen, the maximum size of floatable particles predicted by Eq. (23) is compared with the experimental results despite a number of approximations made during the calculation. A better agreement will be obtained if a higher estimation for ε_{max} is used in the case of the high inputs of energy ($\bar{\varepsilon}$). Nevertheless, the data given in Table 1 for the maximum size of floatable particles is within the range of the observed values in the potash flotation in the industrial scale (Schubert, 1996). In the case of sulphide flotation, Eq. (23) can predict a similar range of $R_{p\ max}$ observed in the industrial scale (Finch, 1979).

The relatively high values of b_m in the *g* unit shown in Table 1 highlight the influence of turbulence on the particle detachment in the flotation process. The particle detachment caused by the particle weight is not as significant as the detachment caused by turbulence, which is the feature of the mechanical cells. In the pneumatic and column cells, turbulence is less intensive but cannot be eliminated completely even with the use of baffles to prevent the backward circulating flows. In these cases, the influence of turbulence on the

particle detachment may be compatible with the influence caused by gravity and many other mechanisms such as shearing and stresses. Clearly, the results obtained so far require further developments for these cases.

7. Conclusion

The stability of particles attached to the gas–liquid interface and its possible detachment were analysed based on the force balance. The simple, yet accurate equations for the maximum size of floatable particle were approximately obtained from the highly nonlinear equations describing the gravity–capillarity coupling phenomena controlling the bubble–particle detachment. The simplified equations were obtained for the tenacity of attachment of particles using the approximate solutions to the Young–Laplace equation. The bubble size has little effect on the tenacity of particle attachment and the upper limit of the particle size. Simple equations for the maximum size of floatable particles were derived as explicit functions of the particle contact angle, the surface tension, the particle density and the mean centrifugal acceleration of the turbulent eddies and were compared with the experimental data. The mean centrifugal acceleration of turbulent eddies is a controlling parameter of the upper size limit of particles to be recovered by flotation in the mechanical cells. It is anticipated that the obtained results can be used for interpreting the flotation results of coarse particles and for modelling the bubble–particle detachment efficiency.

Acknowledgements

The author gratefully acknowledges the Australian Research Council for financial support through a Discovery grant (DP0211085) and Graeme J. Jameson for fruitful discussions.

References

Bischofberger, C., Schubert, H., 1978. Effect of flotation apparatus hydrodynamics on the floatability of various size particles. Freib. Forsch. hefte, A 594, 77–92.

Deglon, D.A., Sawyerr, F., O'Connor, C.T., 1999. A model to relate the flotation rate constant and the bubble surface area flux in mechanical flotation cells. Miner. Eng. 12 (6), 599–608.

Derjaguin, B.V., 1946. Theory of the distortion of a plane surface of a liquid by small objects and its application to the measurement of the contact angle of the wetting of thin filaments and fibres. Dokl. Akad. Nauk SSSR 51 (7), 517–520.

Finch, J.A., 1979. Floatability of coarse galena. Powder Technol. 22, 230–287.

Gaudin, A.M., 1939. Principles of Mineral Processing. McGraw-Hill, New York.

James, D.F., 1974. The meniscus on the outside of a small circular cylinder. J. Fluid Mech. 63 (4), 657–664.

Kabanov, B., Frumkin, A., 1933. Uber die Gross electrolytisch entwickelter Gasblassen. Z. Phys. Chem. (Leipz.) A 165, 433–435.

Nguyen, A.V., 2002. Empirical equations for meniscus depression by particle attachment. J. Colloid Interface Sci. 249, 149–151.

Schubert, H., 1996. Aufbereitung fester Stoffe, Band II, Sortierprozess Deutcher Verlag für Grundstoffindustrie, Stuttgart.

Schubert, H., 1999. On the turbulence-controlled microprocesses in flotation machines. Int. J. Miner. Process. 56 (1–4), 257–276.

Schulze, H.J., 1977. New theoretical and experimental investigation on stability of bubble–particle aggregates in flotation—a theory on upper particle size of floatability. Int. J. Miner. Process. 4, 241–252.

Schulze, H.J., 1980. Zur Berechnung der maximal flotierbaren Korngroess under turbulenten Stroemungsbedingungen am Beispiel von Sylvinit. Neue Bergbautech. 10, 119–121.

Schulze, H.J., 1982. Dimensionless number and approximate calculation of the upper particle size of floatability in flotation machines. Int. J. Miner. Process. 9 (4), 321–328.

Schulze, H.J., 1983. Physico-Chemical Elementary Processes in Flotation. Elsevier, Amsterdam, 320 pp.

Schulze, H.J., 1992. Elements of physically based modelling of the flotation process. NATO ASI Ser., Ser. E: Appl. Sci. (Innovations Flotation Technol.) 208, 171–180.

Wark, I.W., 1933. The physical chemistry of flotation I. J. Phys. Chem. 37, 623–644.